Real-time tracking of ground- and excited-state responses of photoactive molecules to a change of microenvironment, from femtoseconds to milliseconds

Chunyu Li[†,1], Antonio Sampaoli[†,1], Dominik Bäuerle[2], Mariona Bonas Vera[1], Gaëtan Peygourdi[1], Léo Willig[1], John T.M. Kennis[2], Nicoletta Liguori[*,1,2]

[1]ICFO − Institut de Ciències Fotòniques, The Barcelona Institute of Science and Technology, Barcelona 08860, Spain
[2]Department of Physics and Astronomy and Institute for Lasers, Life and Biophotonics, Faculty of Sciences, Vrije Universiteit Amsterdam, de Boelelaan 1081, 1081 HV Amsterdam, The Netherlands

**Corresponding author*
[†]equal contribution

Abstract

Light triggers numerous fundamental biological processes in living organisms, by promoting (multi)chromophoric biomolecular systems to an excited state, which activates their function. The ability of these photoactive systems to absorb and use solar energy is often regulated by their microenvironment, which modulates their structural and energetic landscape and, thus, their functionality. Various stimuli-responsive photoactive materials are designed based on this principle.

Understanding how photoactive molecular systems respond to light and environmental changes requires tracking changes at both the electronically excited- and ground-state levels, with ultrafast resolution across a broad range of timescales. Indeed, while light-induced excited-state dynamics involve processes as rapid as a few femtoseconds, the structural and electrostatic responses to microenvironmental changes may occur at timescales orders of magnitude slower, up to the millisecond and beyond.

We demonstrate that this investigation can now be enabled by a novel and universal three-pulse ultrafast spectroscopy method that: (i) induces controlled, local changes in the microenvironment of a solution, specifically of pH, and (ii) probes the rapid spectroscopic response of photoactive molecules in both the ground and excited states, from femtoseconds to milliseconds. Controlling changes in the microenvironment and – simultaneously – bridging the ultrafast timescales of excited-state dynamics with the slower timescales of environmental and conformational changes is key to advancing our understanding of how living organisms and artificial materials regulate the interplay between light, environment, and structure in light-induced molecular processes.

Photosynthesis, vision, and, more generally, photosensory reception exemplify the capacity of living organisms to capture solar energy and utilize it to activate critical functions. These processes are mediated by photoactive proteins, which typically bind one or multiple chromophores[1–4]. The energy absorbed by the chromophore(s) can be utilized in various ways, *e.g.*, it may be converted into excitations that are then transferred through a network of chromophores to the site of a photochemical reaction, as in the case of photosynthetic light-harvesting complexes[5,6]. Alternatively, it may trigger local changes in ion conductance directly at the level of the protein, as in the case of ion channels and pumps[7–9].

While the activation of photoactive proteins is essential, it may not always confer an advantage to the organism[10–12]. For this reason, living organisms developed strategies to regulate the mechanism of action of their photoactive proteins. In several cases, a critical modulator of the proteins' function is pH[13,14]. For instance, plants and algae developed a mechanism to balance the number of photoexcitations within the photosynthetic membrane, in order to prevent photodamage[15]. To do so, selected proteins from the large family of light-harvesting complexes (LHCs), which are membrane proteins binding chlorophylls and carotenoids[16], can sense pH changes in the lumen of the photosynthetic membrane that are driven by variations in light intensity[17–24]. In response, the LHCs reversibly activate dissipative mechanisms that prevent photodamage under excess sunlight[25–33]. Another example is provided by marine bacteria, in particular the ones that are part of the α-proteobacterial SAR11 clade, which is the most abundant organism in the ocean[34]. These bacteria express rhodopsins, which are retinal-binding membrane proteins[35]. Some of these proteins can tune the duration of their photocycle in response to physiological pH changes, thereby regulating their capacity to transduce signals[36–38]. Their pH-sensitive response has led to the proposal that they could function as sensors of extracellular pH in marine bacteria[36]. Finally, as another example, conformations of opsins with different roles in the visual cycle have also been found to be regulated by pH[39].

The capacity of photoactive proteins to sense and respond to pH has implications that extend beyond biology and has inspired the development of novel light- and stimuli-sensitive nanotechnologies. These include pH-responsive artificial photoactive systems[40–42], pH-dependent assemblies for photodynamic therapy[43–45], and pH-switchable photocatalysts[46–49], among others. Thus, determining the mechanism of response of photoactive proteins to pH changes, step-by-step, can advance our fundamental understanding of the timescales and intermediate steps involved in light- and environment-sensing mechanisms of living organisms. Additionally, it can provide the design principles of functional biomaterials in fields such as drug delivery, artificial photosynthesis, and environmental monitoring.

Several ultrafast tools have been developed to investigate the real-time response of molecular systems to changes of pH[50–56]. The most rapid responses to pH changes at the ground-state level have been tracked via pH-jump time-resolved infrared (IR) spectroscopy[50–53,57,58]. With this method, a laser pulse triggers proton release from either photoacids or caged-protons, into the system of interest. This way a "jump" in the pH of the solution is rapidly obtained, whose magnitude can be tightly controlled[54]. Via synchronized broadband IR pulses, the changes in the ground-state structure of proteins can be probed with a resolution as fast as few femtoseconds (fs)[51,53,57–59].

However, the probing of the pH-driven changes in the function of photoactive systems requires special considerations because it is essential to characterize the intermediate steps in their response to pH at both:

i) the ground-state level, because a pH change might tune the chromophores and the scaffold's structure and electrostatics, in turn modifying the chromophores' network of interactions, structural flexibility, *etc*[23,60–62].

ii) the electronically excited-state level, probing both the optically bright and dark states of the chromophores, because a pH change might result in different excited-state

dynamics with distinct energy transfer efficiencies, pathways, kinetics, and photoproducts, to name a few[20,24,36,40,63,64].
Therefore, determining both light- and environment-driven responses in a single experiment, requires experimental approaches capable of inducing and tracking pH changes and – simultaneously – monitoring the intermediate steps in the changes of the spectroscopic properties of the sample. Such approaches should also maintain fs resolution and probe across timescales spanning several orders of magnitude. Indeed, characterization of the excited-state dynamics requires at least fs resolution[65], while dynamics in the ground state activated by a change of microenvironment might occur at timescales ranging from the (sub)nanosecond (ns)[66–68], *e.g.*, protein conformational changes, up to the milliseconds (ms) and beyond, *e.g.*, changes of protein-protein interactions[69,70].

Here, we tackle this challenge by introducing a universal three-pulse ultrafast spectroscopy method that enables triggering and monitoring changes in the microenvironment, in this case pH, while simultaneously tracking the changes in the spectroscopic properties associated with both the excited and ground state of photoactive molecules, from the femtosecond up to the millisecond. We define the method as *pH-jump Visible Transient Absorption Spectroscopy* or *pH-VISTA.*
The working principles of pH-VISTA are the following:
1) A fs laser pulse (*prepump*) triggers proton release from either a caged proton or a photoacid. As a result, a "pH jump" in the excitation spot is rapidly obtained, whose magnitude can be controlled by tuning experimental parameters[71–73].
2) A second fs pulse (*pump*) excites the photoactive molecular system in the same excitation spot.
3) A third fs white-light supercontinuum pulse (*probe*), detects transient spectra in the excitation spot.
The probe scans at different time delays (~10^{-6}-10^{1} ns) from the pump (τ_{VISTA}), with fs resolution as in standard femtosecond pump-probe spectroscopy[74]. However, the innovation of pH-VISTA lies in the fact that multiple pump-probe datasets can be acquired at different time delays following the initial prepump (τ_{pH}), from the fs to the ms. Such delays span timescales relevant for proton release and transfer (~10^{1}-10^{2} ns[53,75]) and slower dynamics, for example protein conformational changes (~10^{2}-10^{9} ns, depending on the protein[66–68]), capturing – for the first time – their effect on the excited-state dynamics of the photoactive systems. Additionally, since the external excitation source can be alternatively switched on and off during the measurement, as shown below, real-time changes in the absorption spectrum of the photoactive system, while the sample is set in the ground state, are also tracked.

In this work, we demonstrate that pH-VISTA can induce and track a transient pH change in a solution containing a photoactive molecular system and probe – simultaneously – its response at both the excited and ground-state levels. The experiment captures the hierarchy of timescales relevant for determining the intermediate steps in the response of the photoactive system to the change of microenvironment.

Results and Discussion

Experimental settings of pH-VISTA. Bromocresol purple (BCP) was selected as a prototypical pH-sensitive photoactive molecular system. BCP is a pH-sensitive dye widely used as an acid-base indicator[76], coloring yellow at acidic pH levels and purple at basic values (**Figure 1.a**). This pH-dependent change in color is associated with the transition of BCP from the protonated (*sultone*) to the deprotonated (*sulfonate*) form[77]. The concentration profiles of the sultone and sulfonate forms of BCP as a function of pH are illustrated in **Figure 1.b**. BCP was prepared in solution with 2-

nitrobenzaldehyde (2-NBA), which is an irreversible caged-proton source commonly used to trigger pH jumps[52,54,59]. The solution was set at a pH value of 7. Negative-control samples, represented by solutions with BCP or 2-NBA only, were also prepared at the same concentration. Controls were measured in the same conditions and on the same day as the sample containing BCP plus 2-NBA. The setup implemented to develop pH-VISTA is illustrated in **Figure S1** (for details see **Methods**). The prepump was centered at 370 ± 7 nm to excite the 2-NBA, and the pump at 600 ± 5 nm to selectively excite the sulfonate form of BCP (**Figure 1.d**).
Data were collected on a shot-by-shot basis and the prepump, pump, and probe were modulated using a pulse picker (prepump) and choppers (pump, probe). The on/off status of each pulse was monitored by separate photodiodes. At each time step, multiple probe shots were acquired by the detector (in our case 1000 per time step). This shot-by-shot detection and pulse modulation allowed the probe signal recorded at each shot to be assigned to the different on/off statuses of the three pulses. These signals were then combined to generate distinct, relevant types of two-dimensional transient-absorption maps, $\Delta OD(\lambda,\tau)$, all from a single pH-VISTA experiment (**Figure 2**).

Probing the real-time response of a photoactive molecular system to a pH change - at the ground-state level. The $\Delta OD(\lambda,\tau)$ map relevant to capture transient spectroscopic changes in the ground state of BCP following a pH jump, is here defined as *ground-state pH-VISTA* map or *GS-pHVISTA* (**Figure 2**). More in detail, the GS-pHVISTA 2D map, $\Delta OD_{GS-pHVISTA}(\lambda,\tau)$, is computed using signals concomitant with the 600-nm pump being *off*, which is the pump that selectively excites the sulfonate form of BCP. Signals concomitant with the 370-nm prepump being *on* to excite 2-NBA are instead included in the final $\Delta OD_{GS-pHVISTA}(\lambda,\tau)$. The probe is scanned from negative time points up to 0.6 ms with respect to the 370-nm prepump (τ_{pH}).
The $\Delta OD_{GS-pHVISTA}(\lambda,\tau)$ map and its relevant kinetics are reported in **Figure 3.a** and **Figure 3.c**, respectively. In both experiments with either BCP plus 2-NBA or BCP only, ultrafast excited-state dynamics of BCP are observed in the ultrafast timescale (fs to ps), due to the fact that BCP also absorbs the 370-nm prepump, both in its sulfonate and sultone forms (**Figure 1.d**). More in detail, immediately following the 370-nm excitation, a broad negative spectrum is formed in the 520−700 nm range, which is attributed to contributions from ground-state bleach (GSB) and stimulated emission of BCP (**Figure 3.a**). The excited-state dynamics of BCP last on the order of a few ps before it relaxes back to the ground state, as observed in conventional pump-probe measurements on BCP (see **SI** and **Figure S5**). As shown in **Figure 3.a, c**, similar BCP excited-state dynamics are observed in both the presence and absence of 2-NBA upon 370-nm prepump excitation, indicating negligible TA signal contributions from 2-NBA in the spectral region investigated (500-700 nm). This is further confirmed by the negligible $\Delta OD_{GS-pHVISTA}(\lambda,\tau)$ signal of 2-NBA alone over the whole timescale (**Figure 3.a, c**), mainly dominated by a rapid spectral evolution around time zero due to coherent artifacts. Coherent artifacts around time zero are present in all the solutions investigated (2-NBA, BCP, BCP+2-NBA). The lack of effects of 2-NBA on the excited-state dynamics of BCP and the identical absorption spectrum of BCP in the presence and absence of 2-NBA (**Figure 1.d**), indicate that the 2-NBA molecule, *per se*, does not influence the spectroscopic properties of BCP.
Over longer timescales (>>ps), no spectral evolution is observed until the end of the scan, in the solution containing only BCP, indicating that this dye has relaxed to the ground state (**Figure 3.a, c**). However, in the presence of both BCP and 2-NBA, bleach in the range of 500 to 650 nm rises from tens of ns and reaches a maximum at about 15 μs (**Figure 3.c**). These timescales correspond to those previously demonstrated for proton release from 2-NBA after the homolytic cleavage of the nitro group and, by diffusing in the excitation spot, protonation of acceptors in solution.[78,79] Indeed, the

bleach formed in GS-pHVISTA of BCP in the presence of 2-NBA corresponds to the depletion of the BCP sulfonate form, as shown in **Figure S2**. Therefore, considering that over these timescales BCP is in the ground state, as can be inferred from the GS-pHVISTA of BCP alone (**Figure 3.a, c**), the formation of this bleach is due to the protons released from 2-NBA excited by the 370-nm prepump, which induces a pH jump in the excitation spot (**Figure 1.c**).

Finally, due to the combination of the diffusion of protons and protonated BCP outside the excitation spot, and to the continuous circulation of the sample via a peristaltic pump, the bleach gradually decreases to zero. By adjusting the flow rate of the peristaltic pump, the rate at which the bleach is reduced can be regulated (**Figure S3**). However, even at the highest speed of the peristaltic pump employed, the bleach does not fully return to zero within 1 ms. This indicates that, at repetition rates faster than the time required for protons and protonated BCP to clear the excitation spot, each probe shot would be collected with the sample set under different initial pH conditions. To address this potential limit, all our experiments (including the ones presented above) were conducted adopting the following solution: in addition to employing a peristaltic pump to accelerate the diffusion of protons and protonated species outside the excitation spot between shots, a slower modulation was applied to the prepump via a pulse picker, which resulted in a single 370-nm prepump pulse every 11 ms. The 600-nm pump and the probe pulses, instead, were 1-kHz pulses further modulated via mechanical choppers at a rate faster than the prepump, *i.e.*, 125 Hz for pump and 250 Hz for probe, with a 50% duty cycle. This entailed that, during each 10-ms interval in which the 370-nm prepump was “off”, multiple identical “on/off” combinations of the 600-nm pump and the probe were acquired (**Figure 2**). At each time step, 1000 shots were recorded. By using a modulation scheme for the three pulses combined with shot-by-shot detection, we collected enough signals to compute ΔOD(λ,τ) maps, such as the GS-pHVISTA map, while discarding all shots following the 370-nm prepump where the sample had not yet recovered (**Figure S4**).

But, how can the number of shots to be discarded be determined? The $\Delta OD_{GS-pHVISTA}$ signal at negative time points corresponds to timesteps at which the probe arrives before the 370-nm prepump excites the sample, and is here defined as the *pre-zero signal*. In the absence of protons or protonated BCP triggered by a previous 370-nm prepump shot, the intensity of the pre-zero signal is expected to be independent of the number of discarded shots. Therefore, by computing distinct $\Delta OD_{GS-pHVISTA}$ maps, each with an increasing number of shots discarded following the 370-nm prepump, the relationship between the TA signal at negative τ_{pH} delays and the number of discarded shots can be tracked. **Figure S4** illustrates how the pulses are modulated and the shots removed, and shows the experimental dependency of the pre-zero signal intensity plotted as a function of the number of discarded shots. The reported data demonstrate that the pre-zero signal intensity decreases as the number of discarded shots increases, up to 6 shots discarded, and reaches a negligible value at a higher number of discarded shots (**Figure S4.b**). This demonstrates that the peristaltic pump we employed, was capable of refreshing the excitation spot within 6 ms, in our experimental conditions. Overall, we have demonstrated that the combination of: i) sample circulation, ii) pulse modulation along with shot-by-shot detection, and iii) postprocessing by discarding the necessary number of shots after each prepump "on", ensures that the pH-VISTA data are free of artifacts from the accumulation of protons and protonated species, triggered by previous shots.

In summary, we have shown that with pH-VISTA it is possible to trigger a change of pH in the excitation spot and probe the real-time, pH-induced spectroscopic changes of a photoactive molecular system in the ground state, from the femtosecond to the millisecond timescale in a single experiment.

Probing the real-time response of a photoactive molecular system to a pH change - at the excited-state level. To confirm whether pH-VISTA can also monitor real-time, pH-induced changes in the spectroscopic properties of a photoactive molecular system in its excited state, simultaneously to the ground state as described above, the following proof-of-principle experiment was designed.

In the same pH-VISTA experiment used to retrieve the GS-pHVISTA maps, the 600-nm pump was used to excite the sulfonate form of BCP (**Figure 1.d**). The 600-nm pump was kept at a fixed delay of 2 ps with respect to the probe (τ_{VISTA}). At this delay time, BCP is expected to be set in an excited state, as demonstrated via standard pump-probe experiments on BCP upon 600-nm excitation at different pH values, whose results are shown in **Figure S5**. On the other hand, as described above, the probe was scanned from negative time points up to 0.6 ms with respect to the 370-nm prepump (τ_{pH}). Prepump, pump and probe pulses were modulated and the probe spectra were acquired on a shot-by-shot basis (see above).

From the 1000 shots collected at each time step, a conventional pump-probe map, $\Delta OD_{pump-probe}(\lambda,\tau)$, was reconstructed, with the 600-nm pulse being the pump (**Figure 2**). In $\Delta OD_{pump-probe}(\lambda,\tau)$, no difference in signal was found between the solutions containing BCP only or in the presence of 2-NBA, independent of the time delay τ_{pH} from the 370-nm prepump (**Figure S6**), as expected. Indeed, in this 2D map, only signals concomitant with the prepump being off are calculated. Also, the $\Delta OD_{pump-probe}(\lambda,\tau)$, should remain constant along τ_{pH}, because the pump and probe were kept at a fixed delay (2 ps), as indeed observed (**Figure S6**).

Also, with pH-VISTA, an additional pump-probe map can be retrieved. This map is here defined as *excited-state pH-VISTA* or *ES-pHVISTA* map, $\Delta OD_{ES-pHVISTA}(\lambda,\tau)$. ES-pHVISTA is computed by including signals concomitant with the 370-nm prepump on and, additionally and at variance with the GS-pHVISTA, also with the 600-nm pump on (**Figure 2**). The $\Delta OD_{ES-pHVISTA}(\lambda,\tau)$ map along with its relevant kinetics are shown in **Figure 3b**, **d**.

Importantly, in the absence of a pH jump effect, ES-pHVISTA should provide the same information as the conventional $\Delta OD_{pump-probe}(\lambda,\tau)$ map, *i.e.*, a 600-nm pump-probe of the sample investigated (see formulas in **Figure 2**), apart from the multipulse effects in the fs-to-ps timescale of ES-pHVISTA, due to the combination of 370-nm and 600-nm excitations of BCP. These multipulse effects at early time steps were present both in the presence and absence of 2-NBA (**Figure 3d**). However, unlike in conventional $\Delta OD_{pump-probe}(\lambda,\tau)$, a loss of bleach intensity was observed on the order of few tens of ns (τ_{pH}) in the ES-pHVISTA map of BCP plus 2-NBA. The loss of bleach intensity was absent in the case of BCP only, instead. In this case, the bleach remained constant over τ_{pH} as in the case of the conventional $\Delta OD_{pump-probe}(\lambda,\tau)$. The kinetics of GS-pHVISTA and ES-pHVISTA of BCP in the presence of 2-NBA were found to evolve over identical timescales, which are associated to a pH-jump formation and relaxation, as shown in two independent experiments in **Figure 3.c** and **Figure S7.b**. Thus, the loss in the intensity of the ES-pHVISTA in the case of BCP plus 2-NBA was therefore due to the depletion of the sulfonate form of BCP, which is the form responsible for absorbing the 600-nm pump, during the transient acidification of the excitation spot. No ES-pHVISTA signal was observed in the case of 2-NBA alone, as expected due to the lack of excitation of this molecule with a pump set at 600 nm (**Figure 1.d**).

Overall, these experiments demonstrated that in the absence of a pH jump effect, ES-pHVISTA provided the same information as the conventional $\Delta OD_{pump-probe}(\lambda,\tau)$. However, in the case of an actual pH jump, the signals obtained enabled real-time tracking of the pH-induced changes in excited-state dynamics of BCP. Also, within the same experiment, pH-VISTA allowed to relate the pH-driven changes in excite-state dynamics of BCP with the ones in the spectroscopic properties associated to its ground state (**Figure 3.c**).

To comprehensively investigate how the excited-state dynamics of BCP vary in real time in response to a pH change, multiple separate pH-VISTA experiments were run in which τ_{VISTA} was scanned from the fs to the ns as in conventional pump probe, while the time delay between the initial 370-nm prepump and probe was fixed at different τ_{pH} values. As shown in **Figure 4,** and **7.c**, pH-VISTA allowed to retrieve information on the complete excited-state dynamics of BCP at various intermediate pH values and intermediate time steps during the change of pH. The results show that while the excited-state dynamics remain the same at the different pH values, as seen in **Figure S5**, the loss of concentration of the sulfonate form of BCP can be tracked in real time, as in the experiments in **Figure 3.b,c** or **Figure S7.b**, which were run with a τ_{VISTA} fixed at 2 ps. This series of pH-VISTA experiments, with variable τ_{VISTA}, showed that with pH-VISTA, it is possible to collect as many ES-pHVISTA maps as required to analyze the intermediate steps in the pH-response mechanism of any photoactive molecular system of interest, and to capture responses as fast as a few fs and as slow as the (sub)ms (**Figure 5.a**).

Determining the transient change of pH with pH-VISTA. Finally, to correlate the transient changes in the ground- and excited-state spectroscopic properties of BCP with the intermediate values of pH, which is continuously changing along τ_{pH}, we quantified the real-time pH value in the excitation spot by exploiting the relation between the population loss of the 600 nm-excited BCP species and the decrease in pH. Indeed, in a pH-VISTA experiment on BCP, the loss of signal in ES-pHVISTA is given by the depletion of the concentration of the sulfonate form of BCP, which is the species absorbing at 600 nm (**Figure 1.c**). Thus, considering that: i) the pH in the excitation spot at negative time points corresponds to the one of the sample reservoir, which was set at pH 7, and ii) the pH-dependent absorbance of BCP at 600 nm was measured (**Figure S8**), whereas 600 nm is the wavelength used for the pump, the transient pH values as a function of τ_{pH} were determined in **Figure 5.b**. Analysis of the ES-pHVISTA kinetics reveals that, in the experiment using the highest prepump energy per pulse (see Methods and **Figure S7.b**), a maximum 97.2% of total signal was depleted relative to the original signal at negative time points. The 97.2% loss in the amplitude of the photoexcited population of BCP indicated that the pH in the excitation spot was decreased from pH 7.0 to pH 4.7, reaching the highest change of pH on the order of ˜15 microseconds (**Figure S7.b**).

Conclusions

To summarize, we have here introduced a novel, universal three-pulse ultrafast spectroscopy tool that allows to induce, track and quantify a pH change in an excitation spot and simultaneously probe the spectroscopic changes of a photoactive molecular system associated with its ground and excited state, from the femtosecond up to the millisecond timescales. In the proof-of-principle of this novel spectroscopy method, called pH-VISTA, by employing a caged-proton as a proton source, the pH-dependent response of a pH-sensitive dye was monitored in real time, at both the ground- and excited-state level, from the fs to the (sub)ms in a single measurement. Real-time changes in pH were quantified directly from the depopulation of the basic form of BCP, which affected the intensity of excited-state signal. In our experimental conditions, we obtained a maximum pH change from 7.0 to 4.7 in the excitation spot, showing that pH-VISTA is able to induce and track changes of pH relevant to replicate natural physiological processes[39,80].

This methodology, that can be extended to timescales longer than the ms by simply adjusting the repetition rate of the laser (in this case 1 kHz), offers potential applications for studying the real-time response of both natural and artificial photoactive systems in solution. Furthermore, the fs-to-ms three-pulse approach could be extended to implement other types of perturbation, for example by photolysis of caged compounds (*e.g.*, ions, drugs, etc.)[81,82] or inducing temperature changes (*e.g.*,

via near-IR pulses)[83,84], thereby providing versatility for studying the real-time responses of photoactive molecules to various microenvironmental changes, at both the ground- and excited-state levels.

Methods

The pH-VISTA experiments were conducted using a customized dual Yb:KGW regenerative amplified laser system (PHAROS, namely MAIN and SECONDARY, Light Conversion Ltd., 1030 nm, 250 fs, 400 µJ), illustrated in **Figure S1**, at a base repetition rate of 25 kHz. The pulse repetition rate was then reduced by an internal adjustable pulse picker to a final repetition rate of 1 kHz, from both the MAIN and SECONDARY, while maintaining the same energy per pulse. The fundamental 1030 nm output was not directly used in the experiment. A portion (~50%) of the 1030 nm fundamental was used to pump an internal optical parametric amplifier (I-OPA), a rugged module attachable to PHAROS lasers, to generate laser pulses at 800 and 1450 nm (I-OPA signal and idler) from the SECONDARY, and 1450 nm only from the MAIN. The I-OPA idler at 1450 nm was directed into two non-collinear optical parametric amplifiers (both ORPHEUS-N-2H, Light Conversion Ltd.), which were also pumped by the PHAROS 1030 nm, for white light generation. Output from one of the NOPAs (pumped by the MAIN) tuned at 370 nm, referred to as a prepump pulse, was used to excite 2-NBA (8 mM), while the output of the second NOPA (pumped by SECONDARY) at 600 nm (~60 nJ), was used as the pump pulse to excite BCP (8.9 µM, with ~0.06 OD/mm at pH7 at 600 nm).

The output of the I-OPA signal from SECONDARY at 800 nm was used to generate continuum white probe light, by focusing the beam onto a YAG crystal. A set of achromatic lenses was used to collimate the probe continuum before focusing it onto the sample position, and then refocusing it onto the slit of a prism-based spectrometer (Entwicklungsbüro Stresing, Berlin). The shot-by-shot, dispersed probe spectra were recorded on a back-thinned FFT-CCD area image sensor (1024 x 64 pixel, Hamamatsu S12600-1006 model), digitized, and binned, effectively enhancing the signal-to-noise ratio and improving the sensitivity of the sensor, to measure the wavelength-resolved intensity of probe. The prepump and pump pulses were blocked using a beam blocker, after going through the sample.

The time delay between the pump and probe (τ_{VISTA}) was modulated by delaying the pump with an optical delay line, (DL-BKIT2U, Newport) able to scan up to a ˜4-ns delay, with respect to the probe. On the other hand, delays between the prepump and probe (τ_{pH}) were tuned combining an identical optical delay line of the pump (DL-BKIT2U, Newport) with electronic delays. These were obtained by seeding the MAIN and SECONDARY regenerative amplifiers with different pulses from the same oscillator running at a repetition rate of ~75.37 MHz. This entails that the delay between the ejection of pulses from the MAIN and SECONDARY can be controlled electronically with time steps as short as ~13.27 ns (limited by the repetition rate of the oscillator), referred to as electronic delay, following a strategy previously described[85]. Thus, the dual-amplified laser system is therefore capable of scanning delays between the prepump and pump from the fs to 4 ns (with the optical delay line) and from a minimum of ~(13.27 minus 4) ns up to the ms (with the electronic delays). The highest delay possible, in this case 1 ms, is limited by the repetition rate of the prepump and probe, which in our case was set at 1 kHz. In **Figure 4, 5, S2** and **S7**, in order to enhance the pH jump induced by 2-NBA, the optical delay was bypassed to reduce laser power loss, delivering approximately 420 nJ of energy per pulse for the prepump at the sample position. In all other cases, when both optical and electronic delays were used, ~340 nJ per prepump pulse were delivered at the sample position.

To achieve shot-by-shot acquisition and be able to correct for the scattering and background, modulation of the on-off state of prepump, pump and probe pulses as obtained by means of a pulse-picker internal to the NOPA (prepump) and by means of two mechanical choppers (THORLABS) for the pump and probe, synchronized to the

trigger signal from the SECONDARY amplifier. A small fraction of each beam was redirected onto three photodiodes (S1227-66BQ, Hamamatsu) to record the on/off status of the pulses. All photodiodes were connected to a CamControl Unit CC (Stresing FLCC3001-FFT) for the synchronization of the camera and photodiodes.
The shot-by-shot data were recorded and postprocessed via home-built Matlab scripts, to obtain the signals shown in **Figure 2**. Shots corresponding to a sample not yet refreshed between shots, were discarded as explained in **Figure S4**.
Due to the irreversible release of protons, a peristaltic pump was used to refresh the sample between consecutive laser shots. The sample flow was facilitated through a 1-mm quartz flow cell utilizing a peristaltic pump (Watson-Marlow, type 101U/R, 62.0 mL min^{-1}). Meanwhile, the pH value of the reservoir, through which the sample was flown, was monitored by a Fisherbrand accumet Ab150 benchtop pH meter to ensure that the pH of the reservoir would not drift more than 0.1 pH units during the experiment.

References

(1) Mennucci, B.; Corni, S. Multiscale Modelling of Photoinduced Processes in Composite Systems. *Nat Rev Chem* **2019**, *3* (5), 315–330.

(2) Inoue, K. Photochemistry of the Retinal Chromophore in Microbial Rhodopsins. *J Phys Chem B* **2023**, *127* (43), 9215–9222.

(3) Singharoy, A.; Maffeo, C.; Delgado-Magnero, K. H.; Swainsbury, D. J. K.; Sener, M.; Kleinekathöfer, U.; Vant, J. W.; Nguyen, J.; Hitchcock, A.; Isralewitz, B.; Teo, I.; Chandler, D. E.; Stone, J. E.; Phillips, J. C.; Pogorelov, T. V.; Mallus, M. I.; Chipot, C.; Luthey-Schulten, Z.; Tieleman, D. P.; Hunter, C. N.; Tajkhorshid, E.; Aksimentiev, A.; Schulten, K. Atoms to Phenotypes: Molecular Design Principles of Cellular Energy Metabolism. *Cell* **2019**, *179* (5), 1098-1111.e23. https://doi.org/10.1016/J.CELL.2019.10.021.

(4) Croce, R.; van Amerongen, H. Light Harvesting in Oxygenic Photosynthesis: Structural Biology Meets Spectroscopy. *Science (1979)* **2020**, *369* (6506), eaay2058.

(5) Croce, R.; van Amerongen, H. Natural Strategies for Photosynthetic Light Harvesting. *Nat Chem Biol* **2014**, *10* (7), 492–501. https://doi.org/10.1038/nchembio.1555.

(6) Amarnath, K.; Bennett, D. I. G.; Schneider, A. R.; Fleming, G. R. Multiscale Model of Light Harvesting by Photosystem II in Plants. *Proc Natl Acad Sci U S A* **2016**, *113* (5), 1156–1161. https://doi.org/10.1073/pnas.1524999113.

(7) Inoue, K.; Ono, H.; Abe-Yoshizumi, R.; Yoshizawa, S.; Ito, H.; Kogure, K.; Kandori, H. A Light-Driven Sodium Ion Pump in Marine Bacteria. *Nat Commun* **2013**, *4*, 1678.

(8) Nagel, G.; Ollig, D.; Fuhrmann, M.; Kateriya, S.; Musti, A. M.; Bamberg, E.; Hegemann, P. Channelrhodopsin-1: A Light-Gated Proton Channel in Green Algae. *Science (1979)* **2002**, *296* (5577), 2395–2398.

(9) Silapetere, A.; Hwang, S.; Hontani, Y.; Fernandez Lahore, R. G.; Balke, J.; Escobar, F. V.; Tros, M.; Konold, P. E.; Matis, R.; Croce, R. QuasAr Odyssey: The Origin of Fluorescence and Its Voltage Sensitivity in Microbial Rhodopsins. *Nat Commun* **2022**, *13* (1), 5501.

(10) Matuszyńska, A.; Ebenhöh, O. A Reductionist Approach to Model Photosynthetic Self-Regulation in Eukaryotes in Response to Light. *Biochem Soc Trans* **2015**, *43* (6), 1133–1139.

(11) Fain, G. L. Why Photoreceptors Die (and Why They Don't). *Bioessays* **2006**, *28* (4), 344–354.

(12) Müller, P.; Li, X.-P.; Niyogi, K. K. Non-Photochemical Quenching. A Response to Excess Light Energy. *Plant Physiol* **2001**, *125* (4), 1558–1566.

(13) Kovalev, K.; Polovinkin, V.; Gushchin, I.; Alekseev, A.; Shevchenko, V.; Borshchevskiy, V.; Astashkin, R.; Balandin, T.; Bratanov, D.; Vaganova, S.; Popov, A.; Chupin, V.; Büldt, G.; Bamberg, E.; Gordeliy, V. Structure and

Mechanisms of Sodium-Pumping KR2 Rhodopsin. *Sci Adv* **2024**, *5* (4), eaav2671. https://doi.org/10.1126/sciadv.aav2671.
(14) Horton, P.; Ruban, A. V; Walters, R. G. REGULATION OF LIGHT HARVESTING IN GREEN PLANTS. *Annu Rev Plant Biol* **1996**, *47* (Volume 47, 1996), 655–684. https://doi.org/https://doi.org/10.1146/annurev.arplant.47.1.655.
(15) Goss, R.; Lepetit, B. Biodiversity of NPQ. *J Plant Physiol* **2015**, *172*, 13–32. https://doi.org/10.1016/j.jplph.2014.03.004.
(16) Jansson, S. A Guide to the Lhc Genes and Their Relatives in Arabidopsis. *Trends Plant Sci* **1999**, *4* (6), 236–240. https://doi.org/10.1016/S1360-1385(99)01419-3.
(17) Peers, G.; Truong, T. B.; Ostendorf, E.; Busch, A.; Elrad, D.; Grossman, A. R.; Hippler, M.; Niyogi, K. K. An Ancient Light-Harvesting Protein Is Critical for the Regulation of Algal Photosynthesis. *Nature* **2009**, *462* (7272), 518–521. https://doi.org/10.1038/nature08587.
(18) Alboresi, A.; Gerotto, C.; Giacometti, G. M.; Bassi, R.; Morosinotto, T. Physcomitrella Patens Mutants Affected on Heat Dissipation Clarify the Evolution of Photoprotection Mechanisms upon Land Colonization. *Proceedings of the National Academy of Sciences* **2010**, *107* (24), 11128–11133.
(19) Li, X. P.; Björkman, O.; Shih, C.; Grossman, a R.; Rosenquist, M.; Jansson, S.; Niyogi, K. K. A Pigment-Binding Protein Essential for Regulation of Photosynthetic Light Harvesting. *Nature* **2000**, *403* (6768), 391–395. https://doi.org/10.1038/35000131.
(20) Liguori, N.; Roy, L. M.; Opacic, M.; Durand, G.; Croce, R. Regulation of Light Harvesting in the Green Alga Chlamydomonas Reinhardtii: The C-Terminus of LHCSR Is the Knob of a Dimmer Switch. *J Am Chem Soc* **2013**, *135* (49), 18339–18342. https://doi.org/10.1021/ja4107463.
(21) Krishnan-Schmieden, M.; Konold, P. E.; Kennis, J. T. M.; Pandit, A. The Molecular PH-Response Mechanism of the Plant Light-Stress Sensor PsbS. *Nat Commun* **2021**, *12* (1), 1–11.
(22) Bergantino, E.; Segalla, A.; Brunetta, A.; Teardo, E.; Rigoni, F.; Giacometti, G. M.; Szabò, I. Light- and PH-Dependent Structural Changes in the PsbS Subunit of Photosystem II. *Proc Natl Acad Sci U S A* **2003**, *100* (25), 15265–15270. https://doi.org/10.1073/pnas.2533072100.
(23) Liguori, N.; Campos, S.; Baptista, A. M.; Croce, R.; R. R. Campos, S.; Baptista, A. M.; Croce, R.; Nicoletta Liguori, Sara R. R. Campos, António M. Baptista, and R. C. Molecular Anatomy of Plant Photoprotective Switches: The Sensitivity of PsbS to the Environment, Residue by Residue. *J Phys Chem Lett* **2019**, *10* (8). https://doi.org/10.1021/acs.jpclett.9b00437.
(24) Kondo, T.; Pinnola, A.; Chen, W. J.; Dall'Osto, L.; Bassi, R.; Schlau-Cohen, G. S. Single-Molecule Spectroscopy of LHCSR1 Protein Dynamics Identifies Two Distinct States Responsible for Multi-Timescale Photosynthetic Photoprotection. *Nat Chem* **2017**, *9* (8), 772.
(25) Ruban, A. V; Johnson, M. P.; Duffy, C. D. P. The Photoprotective Molecular Switch in the Photosystem II Antenna. *Biochim Biophys Acta* **2012**, *1817* (1), 167–181. https://doi.org/10.1016/j.bbabio.2011.04.007.
(26) Liguori, N.; Xu, P.; Van Stokkum, I. H. M.; Van Oort, B.; Lu, Y.; Karcher, D.; Bock, R.; Croce, R. Different Carotenoid Conformations Have Distinct Functions in Light-Harvesting Regulation in Plants. *Nat Commun* **2017**, *8* (1).
(27) Mascoli, V.; Liguori, N.; Xu, P.; Roy, L. M.; van Stokkum, I. H. M. M.; Croce, R. Capturing the Quenching Mechanism of Light-Harvesting Complexes of Plants by Zooming in on the Ensemble. *Chem* **2019**, *5* (11), 2900–2912.
(28) Ruban, A. V; Berera, R.; Ilioaia, C.; Van Stokkum, I. H. M.; Kennis, J. T. M.; Pascal, A. A.; van Amerongen, H.; Robert, B.; Horton, P.; Van Grondelle, R. Identification of a Mechanism of Photoprotective Energy Dissipation in Higher

Plants. *Nature* **2007**, *450* (7169), 575–578. https://doi.org/10.1038/nature06262.
(29) Müller, M. G.; Lambrev, P.; Reus, M.; Wientjes, E.; Croce, R.; Holzwarth, A. R. Singlet Energy Dissipation in the Photosystem II Light-Harvesting Complex Does Not Involve Energy Transfer to Carotenoids. *Chemphyschem* **2010**, *11* (6), 1289–1296. https://doi.org/10.1002/cphc.200900852.
(30) Ahn, T. K.; Avenson, T. J.; Ballottari, M.; Cheng, Y.-C.; Niyogi, K. K.; Bassi, R.; Fleming, G. R. Architecture of a Charge-Transfer State Regulating Light Harvesting in a Plant Antenna Protein. *Science* **2008**, *320* (5877), 794–797. https://doi.org/10.1126/science.1154800.
(31) de la Cruz Valbuena, G.; VA Camargo, F.; Borrego-Varillas, R.; Perozeni, F.; D'Andrea, C.; Ballottari, M.; Cerullo, G. Molecular Mechanisms of Nonphotochemical Quenching in the LHCSR3 Protein of Chlamydomonas Reinhardtii. *J Phys Chem Lett* **2019**, *10* (10), 2500–2505.
(32) Saccon, F.; Durchan, M.; Bína, D.; Duffy, C. D. P.; Ruban, A. V; Polívka, T. A Protein Environment-Modulated Energy Dissipation Channel in LHCII Antenna Complex. *iScience* **2020**, *23* (9).
(33) Son, M.; Pinnola, A.; Gordon, S. C.; Bassi, R.; Schlau-Cohen, G. S. Observation of Dissipative Chlorophyll-to-Carotenoid Energy Transfer in Light-Harvesting Complex II in Membrane Nanodiscs. *Nat Commun* **2020**, *11* (1), 1–8.
(34) Grote, J.; Thrash, J. C.; Huggett, M. J.; Landry, Z. C.; Carini, P.; Giovannoni, S. J.; Rappé, M. S. Streamlining and Core Genome Conservation among Highly Divergent Members of the SAR11 Clade. *mBio* **2012**, *3* (5), 10–1128.
(35) Rozenberg, A.; Inoue, K.; Kandori, H.; Béjà, O. Microbial Rhodopsins: The Last Two Decades. *Annu Rev Microbiol* **2021**, *75* (1), 427–447.
(36) Kataoka, C.; Sugimoto, T.; Shigemura, S.; Katayama, K.; Tsunoda, S. P.; Inoue, K.; Béjà, O.; Kandori, H. TAT Rhodopsin Is an Ultraviolet-Dependent Environmental PH Sensor. *Biochemistry* **2021**, *60* (12), 899–907.
(37) Sugimoto, T.; Katayama, K.; Kandori, H. Role of Thr82 for the Unique Photochemistry of TAT Rhodopsin. *Biophys Physicobiol* **2021**, *18*, 108–115.
(38) Kataoka, C.; Inoue, K.; Katayama, K.; Béjà, O.; Kandori, H. Unique Photochemistry Observed in a New Microbial Rhodopsin. *J Phys Chem Lett* **2019**, *10* (17), 5117–5121.
(39) Vogel, R.; Siebert, F. Conformations of the Active and Inactive States of Opsin *. *Journal of Biological Chemistry* **2001**, *276* (42), 38487–38493. https://doi.org/10.1074/jbc.M105423200.
(40) Terazono, Y.; Kodis, G.; Bhushan, K.; Zaks, J.; Madden, C.; Moore, A. L.; Moore, T. A.; Fleming, G. R.; Gust, D. Mimicking the Role of the Antenna in Photosynthetic Photoprotection. *J Am Chem Soc* **2011**, *133* (9), 2916–2922. https://doi.org/10.1021/ja107753f.
(41) Reifarth, M.; Bekir, M.; Bapolisi, A. M.; Titov, E.; Nußhardt, F.; Nowaczyk, J.; Grigoriev, D.; Sharma, A.; Saalfrank, P.; Santer, S. A Dual PH-and Light-responsive Spiropyran-based Surfactant: Investigations on Its Switching Behavior and Remote Control over Emulsion Stability. *Angewandte Chemie International Edition* **2022**, *61* (21), e202114687.
(42) Kiskan, B.; Antonietti, M.; Weber, J. Teaching New Tricks to an Old Indicator: PH-Switchable, Photoactive Microporous Polymer Networks from Phenolphthalein with Tunable CO2 Adsorption Power. *Macromolecules* **2012**, *45* (3), 1356–1361.
(43) Qi, T.; Chen, B.; Wang, Z.; Du, H.; Liu, D.; Yin, Q.; Liu, B.; Zhang, Q.; Wang, Y. A PH-Activatable Nanoparticle for Dual-Stage Precisely Mitochondria-Targeted Photodynamic Anticancer Therapy. *Biomaterials* **2019**, *213*, 119219.
(44) Li, F.; Du, Y.; Liu, J.; Sun, H.; Wang, J.; Li, R.; Kim, D.; Hyeon, T.; Ling, D. Responsive Assembly of Upconversion Nanoparticles for PH-activated and Near-infrared-triggered Photodynamic Therapy of Deep Tumors. *Advanced Materials* **2018**, *30* (35), 1802808.

(45) Guan, Q.; Zhou, L.-L.; Li, Y.-A.; Dong, Y.-B. Diiodo-Bodipy-Encapsulated Nanoscale Metal–Organic Framework for Ph-Driven Selective and Mitochondria Targeted Photodynamic Therapy. *Inorg Chem* **2018**, *57* (16), 10137–10145.
(46) Li, R.; Landfester, K.; Ferguson, C. T. J. Temperature-and PH-Responsive Polymeric Photocatalysts for Enhanced Control and Recovery. *Angewandte Chemie* **2022**, *134* (51), e202211132.
(47) Wu, C.; Chen, H.; Corrigan, N.; Jung, K.; Kan, X.; Li, Z.; Liu, W.; Xu, J.; Boyer, C. Computer-Guided Discovery of a PH-Responsive Organic Photocatalyst and Application for PH and Light Dual-Gated Polymerization. *J Am Chem Soc* **2019**, *141* (20), 8207–8220.
(48) Zuo, Q.; Feng, K.; Zhong, J.; Mai, Y.; Zhou, Y. Single-Metal-Atom Polymeric Unimolecular Micelles for Switchable Photocatalytic H2 Evolution. *CCS Chemistry* **2021**, *3* (7), 1963–1971.
(49) Qiu, T.-Y.; Zhao, Y.-N.; Tang, W.-S.; Tan, H.-Q.; Sun, H.-Y.; Kang, Z.-H.; Zhao, X.; Li, Y.-G. Smart Covalent Organic Framework with Proton-Initiated Switchable Photocatalytic Aerobic Oxidation. *ACS Catal* **2022**, *12* (19), 12398–12408.
(50) Baldassarre, M.; Barth, A. The Carbonate/Bicarbonate System as a PH Indicator for Infrared Spectroscopy. *Analyst* **2014**, *139* (9), 2167–2176.
(51) Causgrove, T. P.; Dyer, R. B. Nonequilibrium Protein Folding Dynamics: Laser-Induced PH-Jump Studies of the Helix–Coil Transition. *Chem Phys* **2006**, *323* (1), 2–10.
(52) Donten, M. L.; Hamm, P. PH-Jump Overshooting. *J Phys Chem Lett* **2011**, *2* (13), 1607–1611.
(53) Donten, M. L.; Hassan, S.; Popp, A.; Halter, J.; Hauser, K.; Hamm, P. PH-Jump Induced Leucine Zipper Folding beyond the Diffusion Limit. *J Phys Chem B* **2015**, *119* (4), 1425–1432.
(54) Kohse, S.; Neubauer, A.; Pazidis, A.; Lochbrunner, S.; Kragl, U. Photoswitching of Enzyme Activity by Laser-Induced PH-Jump. *J Am Chem Soc* **2013**, *135* (25), 9407–9411.
(55) Gutman, M.; Huppert, D. Rapid PH and ΔμH+ Jump by Short Laser Pulse. *J Biochem Biophys Methods* **1979**, *1* (1), 9–19.
(56) Mallik, R.; Udgaonkar, J. B.; Krishnamoorthy, G. Kinetics of Proton Transfer in a Green Fluorescent Protein: A Laser-Induced PH Jump Study. *Journal of Chemical Sciences* **2003**, *115* (4), 307–317. https://doi.org/10.1007/BF02704222.
(57) Jeong, B.-S.; Dyer, R. B. Proton Transport Mechanism of M2 Proton Channel Studied by Laser-Induced PH Jump. *J Am Chem Soc* **2017**, *139* (19), 6621–6628.
(58) Flanagan, J. C.; Baiz, C. R. Ultrafast PH-Jump Two-Dimensional Infrared Spectroscopy. *Opt Lett* **2019**, *44* (20), 4937–4940. https://doi.org/10.1364/OL.44.004937.
(59) Donten, M. L.; Hamm, P. PH-Jump Induced α-Helix Folding of Poly-l-Glutamic Acid. *Chem Phys* **2013**, *422*, 124–130.
(60) Navakoudis, E.; Stergiannakos, T.; Daskalakis, V. A Perspective on the Major Light-Harvesting Complex Dynamics under the Effect of PH, Salts, and the Photoprotective PsbS Protein. *Photosynth Res* **2022**, 1–15.
(61) Machuqueiro, M.; Baptista, A. M. Molecular Dynamics at Constant PH and Reduction Potential: Application to Cytochrome c(3). *J Am Chem Soc* **2009**, *131* (35), 12586–12594. https://doi.org/10.1021/ja808463e.
(62) Guarnetti Prandi, I.; Sláma, V.; Pecorilla, C.; Cupellini, L.; Mennucci, B. Structure of the Stress-Related LHCSR1 Complex Determined by an Integrated Computational Strategy. *Commun Biol* **2022**, *5* (1), 145.
(63) Kondo, T.; Gordon, J. B.; Pinnola, A.; Dall'Osto, L.; Bassi, R.; Schlau-Cohen, G. S. Microsecond and Millisecond Dynamics in the Photosynthetic Protein

LHCSR1 Observed by Single-Molecule Correlation Spectroscopy. *Proceedings of the National Academy of Sciences* **2019**, *116* (23), 11247–11252.
(64) Hontani, Y.; Ganapathy, S.; Frehan, S.; Kloz, M.; De Grip, W. J.; Kennis, J. T. M. Strong PH-Dependent near-Infrared Fluorescence in a Microbial Rhodopsin Reconstituted with a Red-Shifting Retinal Analogue. *J Phys Chem Lett* **2018**, *9* (22), 6469–6474.
(65) Maiuri, M.; Garavelli, M.; Cerullo, G. Ultrafast Spectroscopy: State of the Art and Open Challenges. *J Am Chem Soc* **2020**, *142* (1), 3–15. https://doi.org/10.1021/jacs.9b10533.
(66) Chung, H. S.; Khalil, M.; Smith, A. W.; Ganim, Z.; Tokmakoff, A. Conformational Changes during the Nanosecond-to-Millisecond Unfolding of Ubiquitin. *Proc Natl Acad Sci U S A* **2005**, *102* (3), 612–617.
(67) Liguori, N.; Periole, X.; Marrink, S. J.; Croce, R. From Light-Harvesting to Photoprotection: Structural Basis of the Dynamic Switch of the Major Antenna Complex of Plants (LHCII). *Sci Rep* **2015**, *5*, 15661. https://doi.org/10.1038/srep15661.
(68) Balakrishnan, G.; Weeks, C. L.; Ibrahim, M.; Soldatova, A. V; Spiro, T. G. Protein Dynamics from Time Resolved UV Raman Spectroscopy. *Curr Opin Struct Biol* **2008**, *18* (5), 623–629.
(69) Daskalakis, V.; Papadatos, S.; Kleinekathöfer, U. Fine Tuning of the Photosystem II Major Antenna Mobility within the Thylakoid Membrane of Higher Plants. *Biochimica et Biophysica Acta (BBA)-Biomembranes* **2019**, 183059.
(70) Wassenaar, T. A.; Pluhackova, K.; Moussatova, A.; Sengupta, D.; Marrink, S. J.; Tieleman, D. P.; Böckmann, R. A. High-Throughput Simulations of Dimer and Trimer Assembly of Membrane Proteins. The DAFT Approach. *J Chem Theory Comput* **2015**, *11* (5), 2278–2291. https://doi.org/10.1021/ct5010092.
(71) Jeong, B.-S.; Dyer, R. B. Proton Transport Mechanism of M2 Proton Channel Studied by Laser-Induced PH Jump. *J Am Chem Soc* **2017**, *139* (19), 6621–6628. https://doi.org/10.1021/jacs.7b00617.
(72) Kohse, S.; Neubauer, A.; Pazidis, A.; Lochbrunner, S.; Kragl, U. Photoswitching of Enzyme Activity by Laser-Induced PH-Jump. *J Am Chem Soc* **2013**, *135* (25), 9407–9411. https://doi.org/10.1021/ja400700x.
(73) Donten, M. L.; Hamm, P. PH-Jump Overshooting. *J Phys Chem Lett* **2011**, *2* (13), 1607–1611. https://doi.org/10.1021/jz200610n.
(74) Berera, R.; van Grondelle, R.; Kennis, J. T. M. Ultrafast Transient Absorption Spectroscopy: Principles and Application to Photosynthetic Systems. *Photosynth Res* **2009**, *101* (2), 105–118. https://doi.org/10.1007/s11120-009-9454-y.
(75) Donten, M. L.; Hamm, P.; VandeVondele, J. A Consistent Picture of the Proton Release Mechanism of o NBA in Water by Ultrafast Spectroscopy and Ab Initio Molecular Dynamics. *J Phys Chem B* **2011**, *115* (5), 1075–1083.
(76) Yao, W.; Byrne, R. H. Spectrophotometric Determination of Freshwater Ph Using Bromocresol Purple and Phenol Red. *Environ Sci Technol* **2001**, *35* (6), 1197–1201. https://doi.org/10.1021/ES001573E/ASSET/IMAGES/MEDIUM/ES001573EE00020.GIF.
(77) Yao, W.; Byrne, R. H. Spectrophotometric Determination of Freshwater PH Using Bromocresol Purple and Phenol Red. *Environ Sci Technol* **2001**, *35* (6), 1197–1201. https://doi.org/10.1021/es001573e.
(78) Donten, M. L.; Hamm, P. PH-Jump Induced α-Helix Folding of Poly-l-Glutamic Acid. *Chem Phys* **2013**, *422*, 124–130. https://doi.org/https://doi.org/10.1016/j.chemphys.2012.11.023.
(79) Donten, M. L.; Hassan, S.; Popp, A.; Halter, J.; Hauser, K.; Hamm, P. PH-Jump Induced Leucine Zipper Folding beyond the Diffusion Limit. *J Phys Chem B* **2015**, *119* (4), 1425–1432. https://doi.org/10.1021/jp511539c.

(80) Takizawa, K.; Cruz, J. A.; Kanazawa, A.; Kramer, D. M. The Thylakoid Proton Motive Force in Vivo. Quantitative, Non-Invasive Probes, Energetics, and Regulatory Consequences of Light-Induced Pmf. *Biochimica et Biophysica Acta (BBA)-Bioenergetics* **2007**, *1767* (10), 1233–1244.
(81) Xiong, H.; Xu, Y.; Kim, B.; Rha, H.; Zhang, B.; Li, M.; Yang, G.-F.; Kim, J. S. Photo-Controllable Biochemistry: Exploiting the Photocages in Phototherapeutic Window. *Chem* **2023**, *9* (1), 29–64. https://doi.org/10.1016/j.chempr.2022.11.007.
(82) Ellis-Davies, G. C. R. Useful Caged Compounds for Cell Physiology. *Acc Chem Res* **2020**, *53* (8), 1593–1604. https://doi.org/10.1021/acs.accounts.0c00292.
(83) Chung, H. S.; Khalil, M.; Smith, A. W.; Tokmakoff, A. Transient Two-Dimensional IR Spectrometer for Probing Nanosecond Temperature-Jump Kinetics. *Review of Scientific Instruments* **2007**, *78* (6), 63101.
(84) Cerminara, M. Fast-Folding Kinetics Using Nanosecond Laser-Induced Temperature-Jump Methods BT - Protein Folding: Methods and Protocols; Muñoz, V., Ed.; Springer US: New York, NY, 2022; pp 117–134. https://doi.org/10.1007/978-1-0716-1716-8_6.
(85) Konold, P. E.; van Stokkum, I. H. M.; Muzzopappa, F.; Wilson, A.; Groot, M.-L.; Kirilovsky, D.; Kennis, J. T. M. Photoactivation Mechanism, Timing of Protein Secondary Structure Dynamics and Carotenoid Translocation in the Orange Carotenoid Protein. *J Am Chem Soc* **2019**, *141* (1), 520–530. https://doi.org/10.1021/jacs.8b11373.
(86) Martin, M. M.; Plaza, P.; Meyer, Y. H. Transient Spectroscopy of Triphenylmethane Derivatives Following Subpicosecond Irradiation. *Chem Phys* **1991**, *153* (1), 297–303. https://doi.org/https://doi.org/10.1016/0301-0104(91)90025-O.
(87) Biswas, C.; Rao Soma, V.; Chetti, P.; Santosh Kumar Raavi, S. Ultrafast Excited State Relaxation Dynamics of New Fuchsine- a Triphenylmethane Derivative Dye. *ChemPhysChem* **2021**, *22* (24), 2562–2572. https://doi.org/https://doi.org/10.1002/cphc.202100562.

Supporting Information
Additional results and methods.

Acknowledgments
The authors are grateful to Bart van Oort, Vincenzo Mascoli and Antonio Liguori for critical advices and to Mathesh Vaithiyanathan, Judit Donada and Ashfaq Ahammed for their help in the initial phases of the project. The authors would also like to thank the Electronic and Mechanical workshops of ICFO and the Vrije Universiteit Amsterdam for their technical assistance during the implementation of the setup.

Funding:
Dutch Research Council (NWO) grant VENI (**NL**)
The project that gave rise to these results received the support of a fellowship from “la Caixa” Foundation (ID 100010434). The fellowship code is LCF/BQ/PI22/11910032 (**NL**)
This work was partly funded by a BIST Ignite Programme grant from the Barcelona Institute of Science and Technology - Project NANOLYMPICS (**NL**)
This work was partially funded by CEX2019-000910-S [MCIN/ AEI/10.13039/501100011033] (**AS**)
La ayuda JDC2022-049604-I, financiada por MCIN/AEI/10.13039/501100011033 y por la Unión Europea “NextGenerationEU”/PRTR (**CL**)
Funded by the European Union (Light4Switch, 101152468). (**CL**) Views and opinions expressed are however those of the author(s) only and do not necessarily reflect those

of the European Union or European Research Executive Agency. Neither the European Union nor the granting authority can be held responsible for them.
Dutch Research Council (NWO) grants VICI and Middelgroot investment (**JTMK**)

Competing interests: Authors declare that they have no competing interests.

Data and materials availability: All data used in this work are presented in the main text and supplementary material and there is no restriction on data availability.

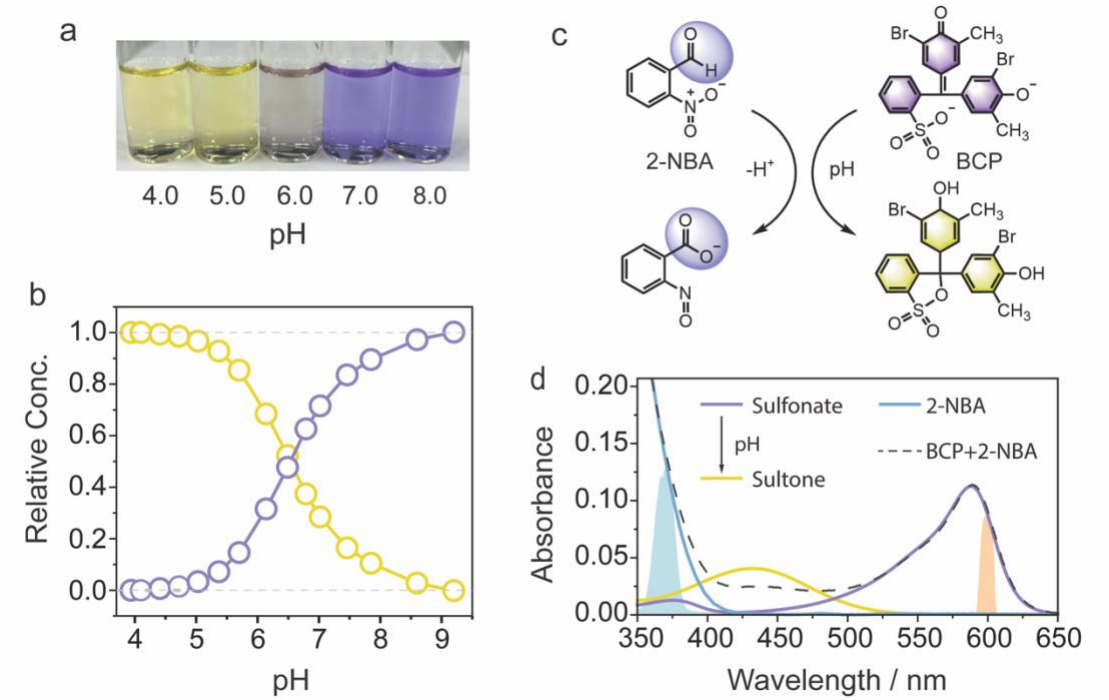

Figure 1. a) Colour change in a solution of BCP, as pH ranges from 4.0 to 8.0; **b)** Relative-concentration profiles of the sultone (yellow line) and sulfonate (violet line) forms of BCP, measured at different pH values at a concentration of 10 µM. The figure was constructed by fitting c1(pH) and c2(pH) using the Beer-Lambert law with theoretical extinction coefficients and measured absorption values at different pH values (as in **Figure S8**), by imposing the condition c1+c2 = 1; **c)** Illustration of the transition of BCP from a sulfonate to a sultone, protonated form, triggered by the proton release from 2-NBA upon a prepump excitation; **d)** UV−Vis absorption spectra of BCP (10 µM) in water at pH 3.9 (yellow line) and 9.2 (violet line), representing the sultone and sulfonate forms respectively, as well as 2−NBA in water (8 mM) and with BCP. The 370-nm prepump and 600-nm pump pulse spectra are depicted with blue and orange-shaded curves.

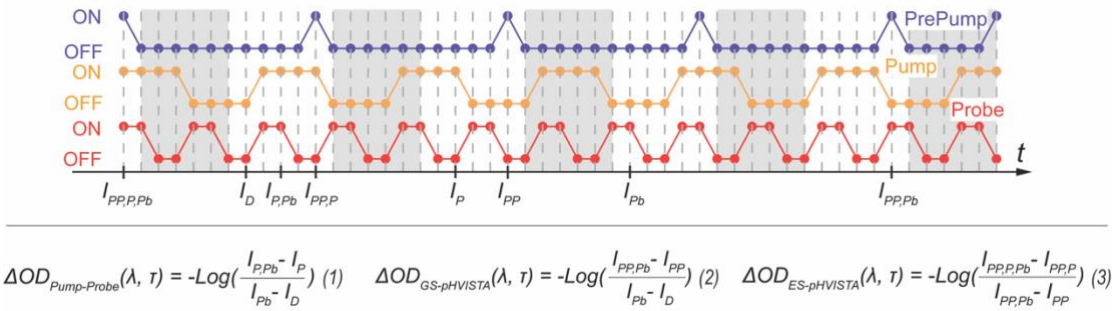

$$\Delta OD_{Pump\text{-}Probe}(\lambda, \tau) = -Log\left(\frac{I_{P,Pb} - I_P}{I_{Pb} - I_D}\right) \quad (1)$$

$$\Delta OD_{GS\text{-}pHVISTA}(\lambda, \tau) = -Log\left(\frac{I_{PP,Pb} - I_{PP}}{I_{Pb} - I_D}\right) \quad (2)$$

$$\Delta OD_{ES\text{-}pHVISTA}(\lambda, \tau) = -Log\left(\frac{I_{PP,P,Pb} - I_{PP,P}}{I_{PP,Pb} - I_{PP}}\right) \quad (3)$$

Figure 2. Illustration of a shot-by-shot sequence of prepump (PP), pump (P) and probe (Pb) shots (51 shots shown in this example), representative of the ones recorded by the three photodiodes after modulation of the pulses via a pulse picker (prepump) and choppers (pump and probe). The solid circles indicate the status of the pulses (on/off). The probe signal is dispersed via a prism and also recorded on a shot-by-shot basis. In post-processing, the contribution of the 6 shots consequent to each prepump "ON" (shaded area) is not considered in the final dataset, to avoid artifacts caused by the incomplete refreshment of the excitation spot (**Figure S4**). Examples of signal definitions are presented at the bottom (*e.g.,* PP "ON", P "ON", Pb "ON" = $I_{PP,P,Pb}$). The lower panel indicates the formulas used to calculate conventional pump probe (1), GS-pHVISTA (2) and ES-pHVISTA (3).

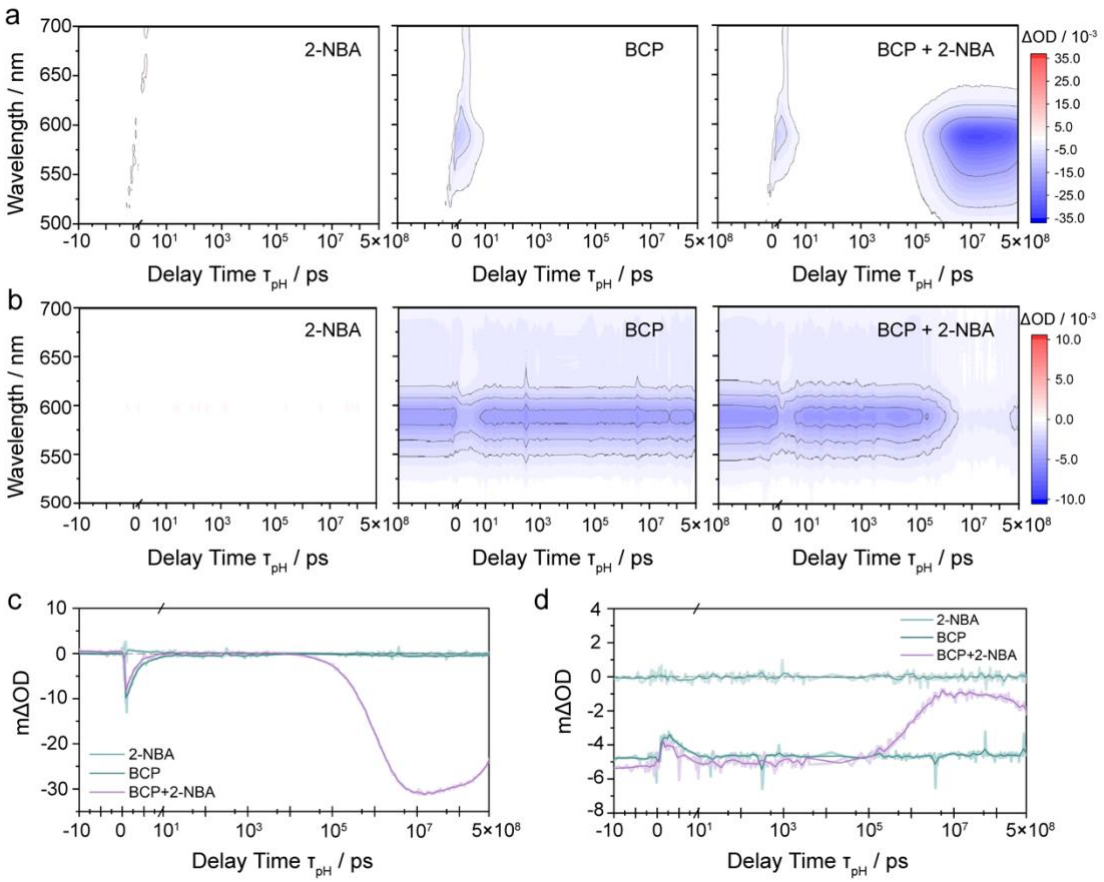

Figure 3. a) GS-pHVISTA and **b)** ES-pHVISTA from 2-NBA (left panel), BCP only (middle panel), and BCP plus 2-NBA (right panel), collected at a fixed pump-probe delay of 2 ps (τ_{VISTA}). In this pH-VISTA experiment, both the optical delay line and electronic long delays were used to scan along τ_{pH}. Data averaged every 4 time steps for clarity. **c)** GS-pHVISTA kinetics of the three different samples at the minimum of the BCP bleach (589 nm). **d)** ES-pHVISTA kinetics of the three different samples also at 589 nm. In **c)** and **d)**, solid lines represent the signals averaged over each 4 time steps.

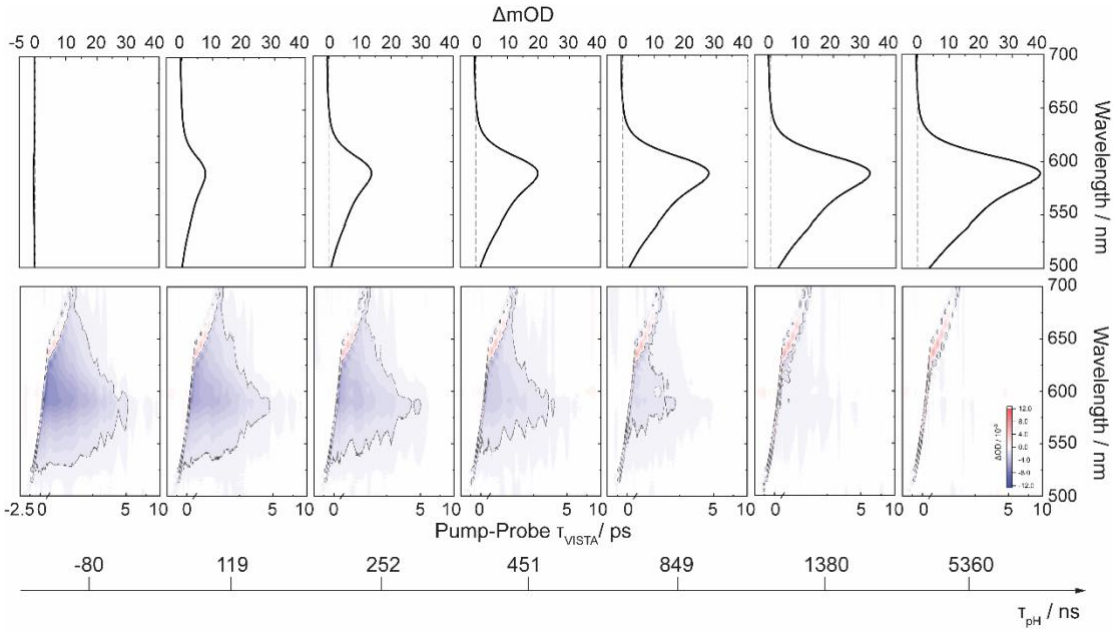

Figure 4. GS-pHVISTA spectra (upper panel) and ES-pHVISTA (bottom panel) with variable pump-probe delay, τ_{VISTA} (averaged every 4 timesteps) of BCP in the presence of 8mM 2-NBA, at selected prepump delay times τ_{pH}. In this figure, per each complete scan along τ_{VISTA}, τ_{pH} was kept fixed at a selected value, as indicated on the time line at the bottom. T_{VISTA} was varied from the fs up to 10 ps.

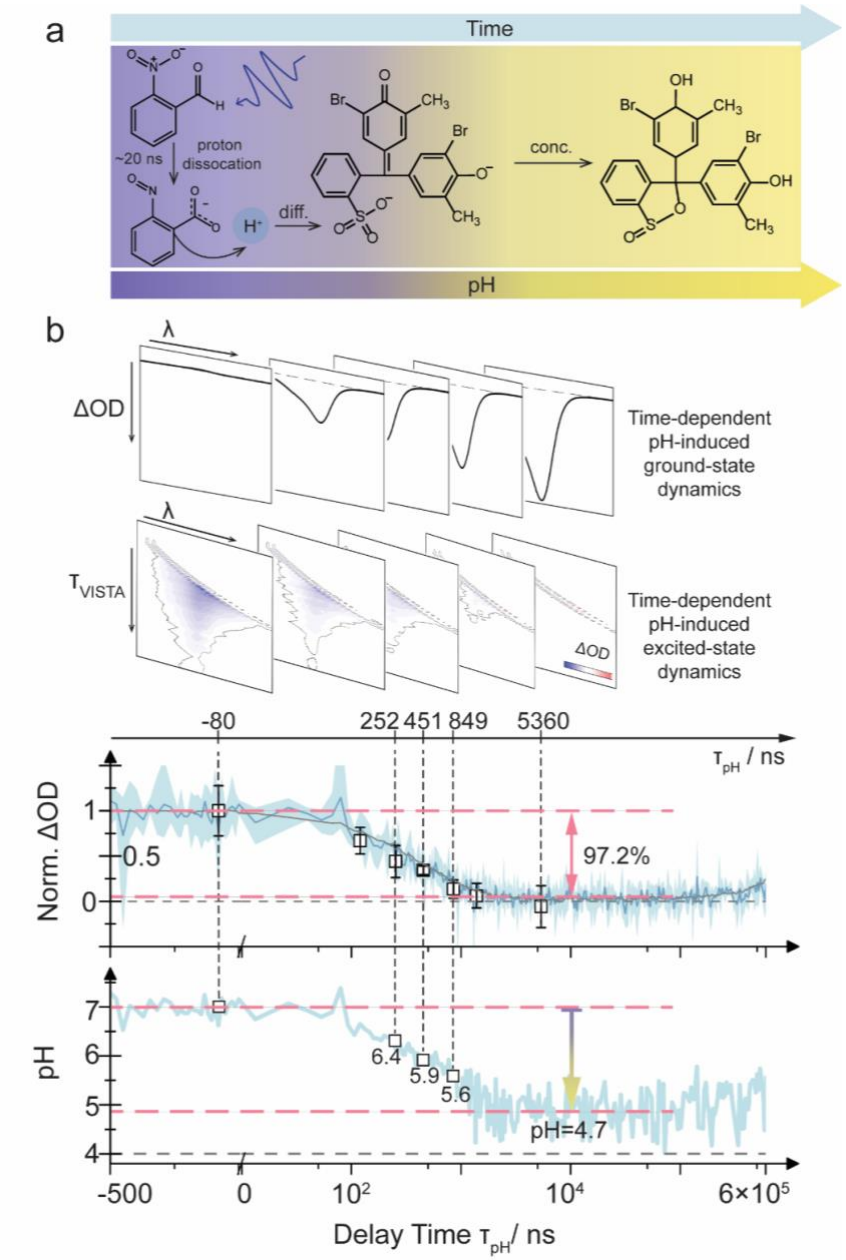

Figure 5. a) Schematic of the photochemistry induced and probed with pH-VISTA on a system composed of 2-NBA (caged-proton) and a pH-sensitive photoactive system (BCP). **b) Top:** Time-dependent series of the absorption spectra and pump-probe spectra of BCP, following a pH jump. The 2D maps shown are representative data selected from **Figure 4**. **Middle:** Time-dependent GS- and ES-pHVISTA signals at 589 nm of BCP plus 2-NBA, in blue and gray, respectively, both averaged over 5 scans. The shaded area marks the standard error over the 5-scan average for the ES-pHVISTA signal. **Bottom:** conversion of the ES-pHVISTA loss of bleach amplitude (indicated above by the pink arrow and dashed lines to be 97.2%) into the change of pH in the excitation spot (see main text and **Figure S8**).

Supporting Information

Real-time tracking of ground- and excited-state responses of photoactive molecules to a change of microenvironment, from femtoseconds to milliseconds

Chunyu Li[†,1], Antonio Sampaoli[†,1], Dominik Bäuerle[2], Mariona Bonas Vera[1], Gaëtan Peygourdi[1], Léo Willig[1], John T.M. Kennis[2], Nicoletta Liguori[*,1,2]

[1]ICFO − Institut de Ciències Fotòniques, The Barcelona Institute of Science and Technology, Barcelona 08860, Spain
[2]Department of Physics and Astronomy and Institute for Lasers, Life and Biophotonics, Faculty of Sciences, Vrije Universiteit Amsterdam, de Boelelaan 1081, 1081 HV Amsterdam, The Netherlands

**Corresponding author*
[†]equal contribution

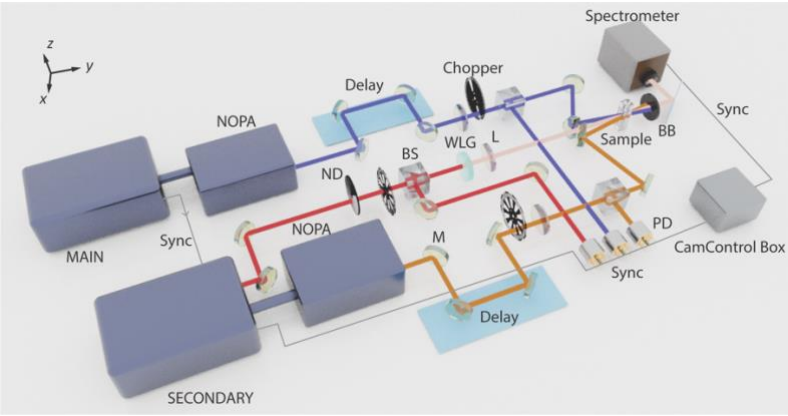

Figure S1. Scheme of the pH-VISTA setup built at ICFO. The acronyms indicate the following: NOPA non-collinear optical parametric amplifier, ND neutral density filter, BS beamsplitter, WLG white light generation, L lens, M mirror, PD photodiode, BB beam blocker; Prepump is purple, pump is orange and probe is light pink.

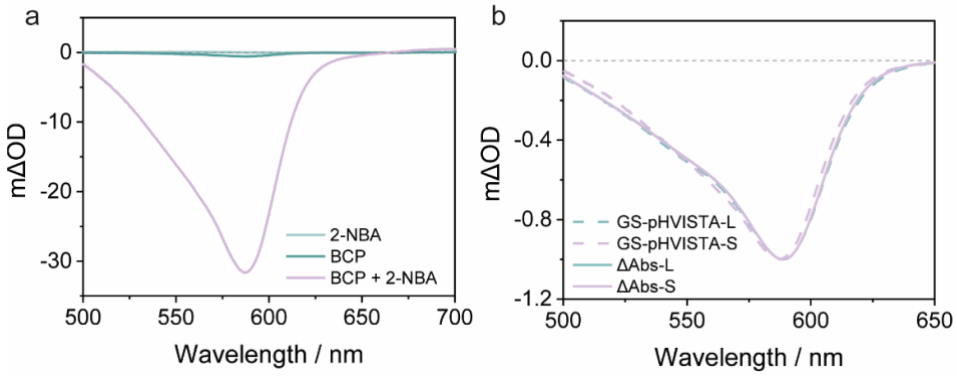

Figure S2. (a) GS-pHVISTA spectrum in different conditions (as indicated in the legend) integrated between 10 and 30 μs; (b) Normalized GS-pHVISTA spectrum of BCP with 2-NBA measured with (S) and without (L) the optical delay line (dashed lines), plotted together with the differential steady-state absorption spectra (ΔAbs) corresponding to the pH change in the (S) and (L) cases, respectively. The ΔAbs were computed from the experimental titration shown in **Figure S8**, by subtracting the absorption spectra at pH 4.7 (L case) or pH 5.2 (S case) from the one at pH 7 - pH of the bulk sample solution and, therefore, initial pH before the jump in both experiments.

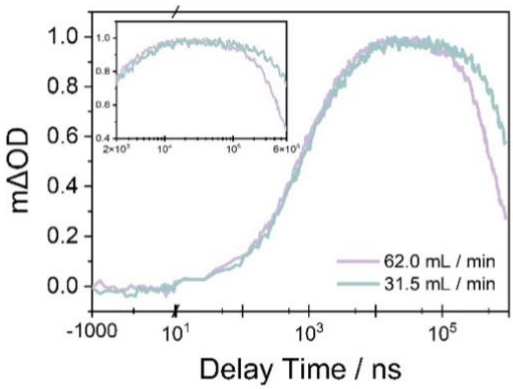

Figure S3. The normalized kinetics of GS-pHVISTA centered at 589 nm of BCP plus 2-NBA, under different peristaltic pump flow rates.

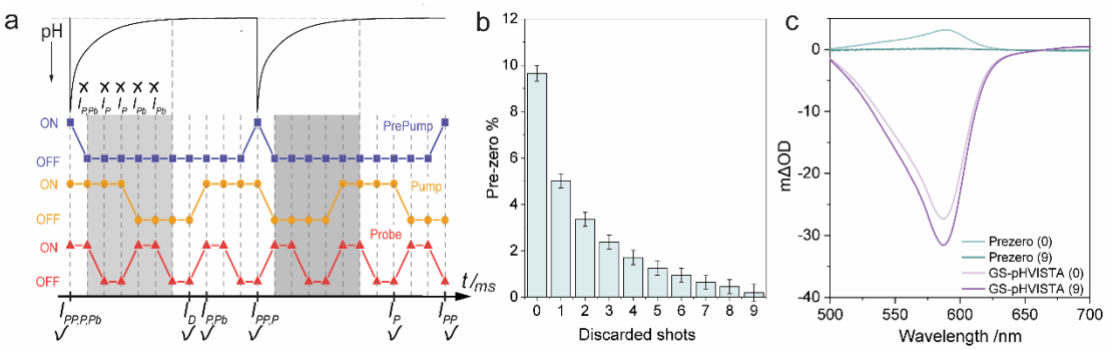

Figure S4. a) Schematic illustration of the pH-jump and identity of shots discarded to eliminate the pre-zero signals. **b)** Ratio between pre-zero signal intensity (τ_{pH} from -1.3μs to 256 ns) and the maximum of the GS-pHVISTA bleach (τ_{pH} from 10μs to 30μs) at 589nm, as a function of the number of discarded shots. Error bars represent the standard error with respect to the average of 5 scans. Data from the experiment shown in **Figure 3** on BCP + 2-NBA. c) The spectra of pre-zero signal and GS-pHVISTA at 0 and 9 discarded shots.

Standard pump-probe experiments on BCP at different pH values. To elucidate how the excited-state dynamics of BCP depend on pH, pump-probe spectra were acquired at different fixed pH values (5.0, 5.5, 6.0, 6.5, and 7.0), while maintaining the same BCP concentration (see **Methods**), in a conventional pump-probe experiment (**Figure S5a**). The pump was centered at 600 nm, as in pH-VISTA. Following excitation, a broad negative signal in the $\Delta OD_{pump-probe}$ spectrum appears in the 520−700 nm range, representing the ground-state bleach (GSB) (**Figure S5b**), along with an overlapping signal in the 600−800 nm spectral region associated with stimulated emission (SE) (as can be inferred from BCP emission in **Figure S9**). By further increasing the delay (~4 to 15 ps), the intensity of the SE band diminishes and an excited-state absorption band becomes more evident in the range ~610-625 nm (**Figure S5b**). The overall signal decays significantly within the first 30 ps. The pH-dependent normalized $\Delta OD_{pump-probe}$ spectra at 2 ps, as well as the normalized kinetics, were found to be identical across all the pH levels tested (**Figure S5c** and **S5d**). However, the amplitude of the pump-probe ΔOD signal was shown to vary with pH, as it could be expected from the pH-dependent concentration of sulfonate, which is the BCP form that absorb the 600-nm pump (**Figure 1**). By normalizing the $\Delta OD_{pump-probe}$ intensity at 580 nm at 2 ps to the value measured at pH 7, and then by calculating the relative ratios of intensities at the other pH levels against this reference, the same relative signal loss was found to occur in both pump-probe and pH-dependent steady-state absorption measurements[86,87]. In the steady-state absorption

measurements, the absorption at 589 nm at pH 7 was used as a reference, and the changes at other pH levels are expressed as relative ratios to this baseline. This consistency implies that the change in amplitude of the ES-pHVISTA at 589 nm can serve as a quantitative method for assessing pH in the context of BCP (**Figure 5**), as no other pH-dependent changes are expected to take place at the level of its excited-state dynamics.

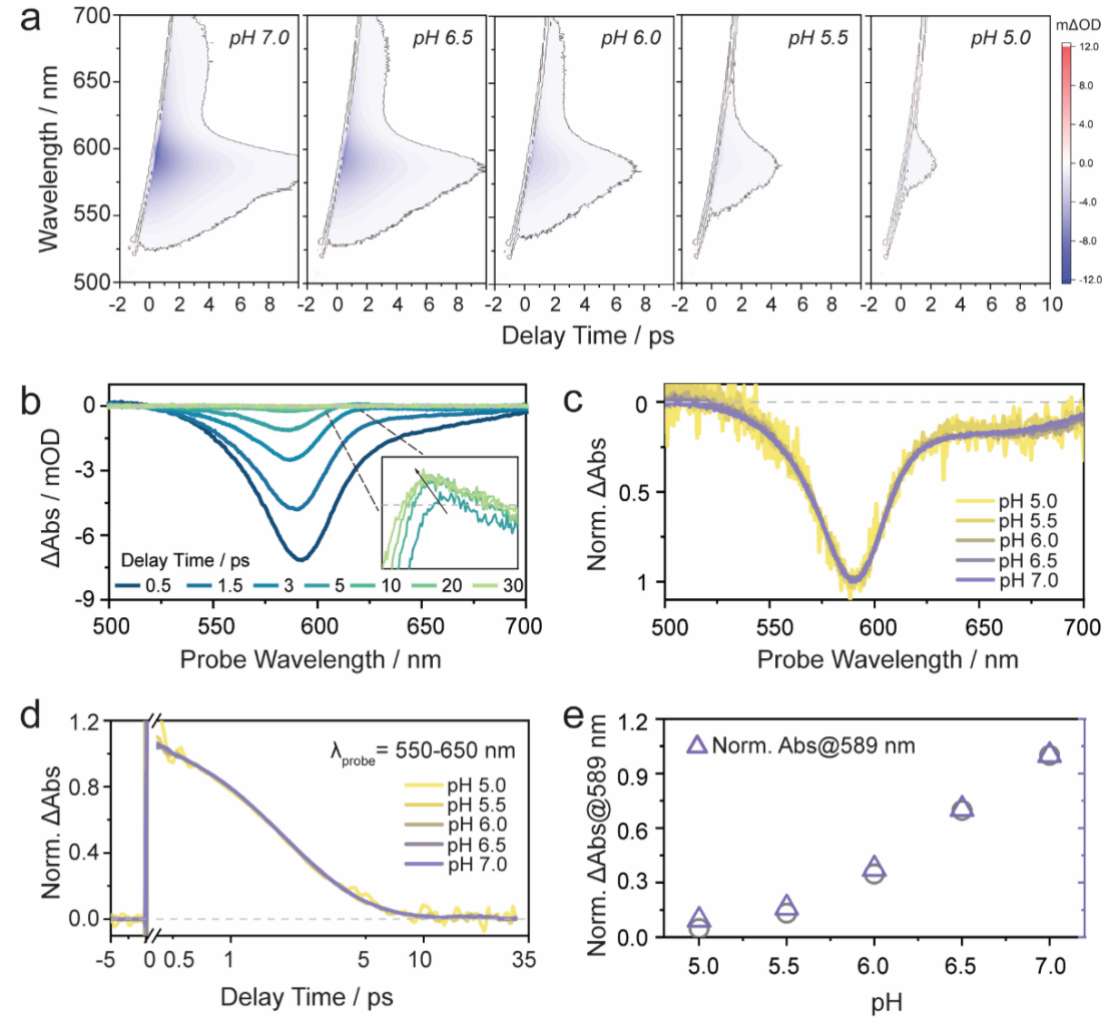

Figure S5. a) $\Delta OD_{pump-probe}$ maps of aqueous BCP solutions at varying pH, upon 600-nm pump excitation. Maps averaged every 4 timesteps. **b)** Representative $\Delta OD_{pump-probe}$ spectra of BCP at pH 7.0, at selected delay times. **c)** Normalized TA spectrum of BCP at 2 ps, at various pH values; **d)** Normalized $\Delta OD_{pump-probe}$ kinetics of BCP, obtained by integrating between 550 and 650 nm. **e)** The dependence of steady-state absorption at 589 nm (right axis, purple triangle) versus $\Delta OD_{pump-probe}$ intensity at 589 nm (left axis, gray circle), at various pH, calculated as described in the section above.

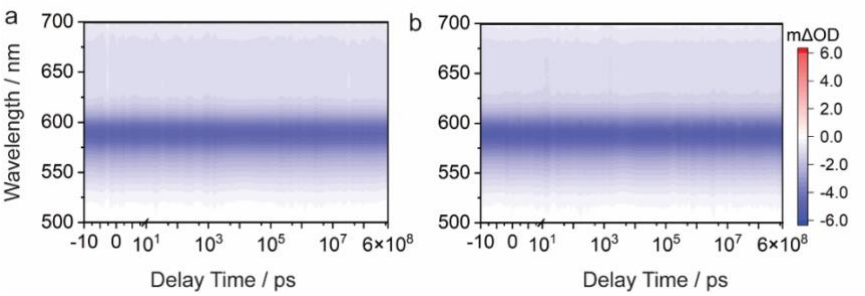

Figure S6. $\Delta OD_{pump-probe}$ maps of BCP in the absence of 2-NBA (**a**) and in the presence of 2-NBA (**b**), from the same experiments shown in **Figure 3**. Both maps are obtained during a pH-VISTA experiment, by scanning the delays along τ_{pH} employing both the optical delay line and electronic long delays, while maintaining τ_{VISTA} at the fixed time step of 2 ps. For $\Delta OD_{pump-probe}$ formula see main text and **Figure 2**, **S7.a**.

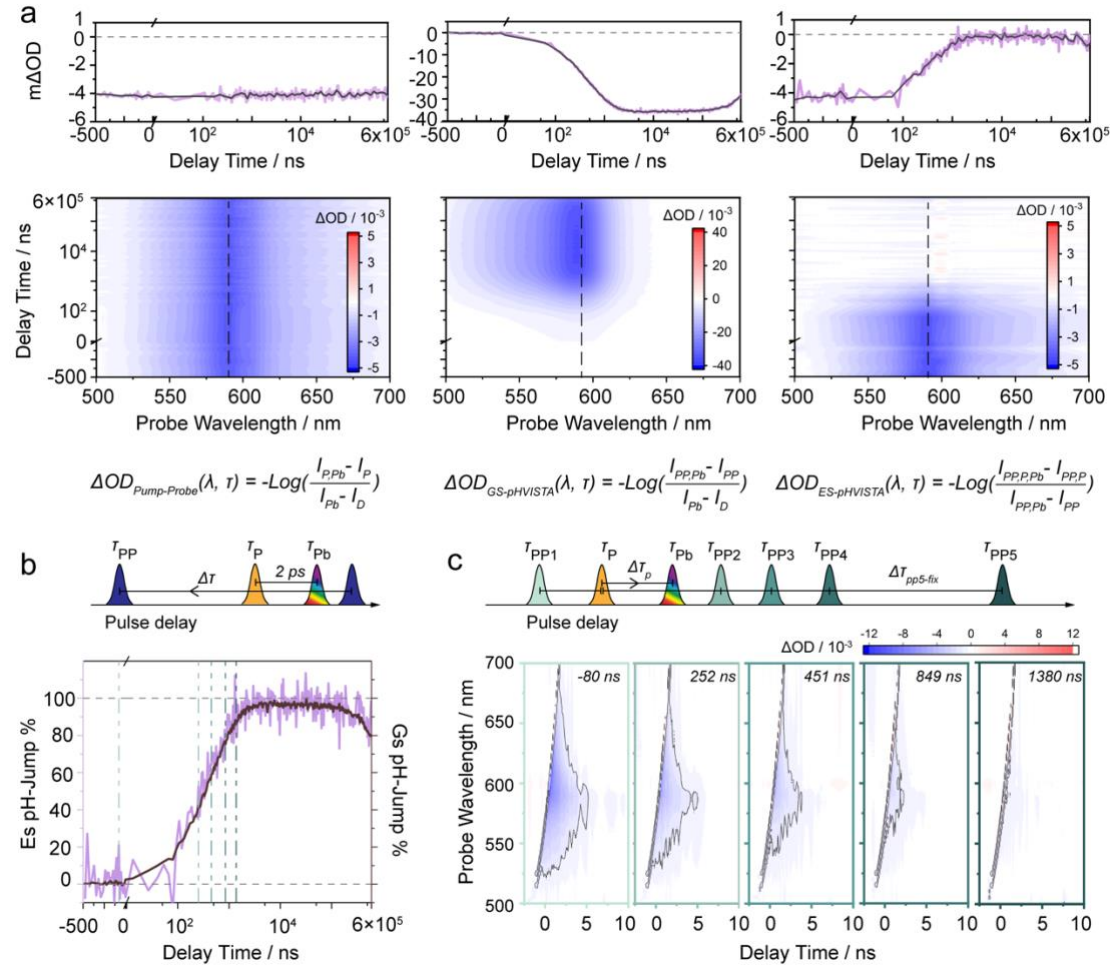

Figure S7. a) Two−dimensional maps of $\Delta OD_{pump-probe}$ (left panel), GS-pHVISTA (middle panel), and ES-pHVISTA (right panel) of BCP aqueous solutions in the presence of 2−NBA averaged each 4 timesteps, from the same experiments shown in **Figure 5**. The respective kinetics at 589 nm are shown above the maps (raw data in lilac, averaged every 4 timesteps in gray). The formulas used to compute each map are reported at the bottom, and in **Figure 2**. **b)** From the same experiments, the kinetics at 589 nm of ES-pHVISTA (lilac) and GS-pHVISTA (black) are normalized for comparison. An illustration of the sequence of pulses used in the experiment is shown above. **c)** ES-pHVISTA maps collected on the same day of the experiment in **a,b**, but varying τ_{VISTA} to collect each ES-pHVISTA map at different, fixed τ_{pH} values. All maps are averaged every 4 timesteps for clarity. An illustration of the sequence of pulses used in the experiment is shown above.

pH titration of BCP. An aqueous stock solution of 150 mL bromocresol purple at 10 µM was prepared from fresh powder, using distilled water. This was then split into three separate solutions of 50 mL, one of which directly served for titration in the pH range of 3.8-5.3 and at pH 9.2. To the other two solutions, 1 mM concentrations of a buffer were added, being either 4-(2-Hydroxyethyl)-1-piperazine ethanesulfonic acid (HEPES), for samples in pH range 6.8-8.2, or 2-(4-morpholinyl)ethanesulfonic acid (MES), for the samples in the pH 5.5-6.7 range. Volumes of a few µL 10M NaOH or 3M HCl were added to adjust pH with negligible dilution effects, and absorption measurements were taken directly after pH measurement with a Fisherbrand™ accumet™ AB150 Benchtop pH Meter, using automated temperature correction. A Varian Cary 4000 UV-Vis-spectrophotometer was used to acquire the absorption spectra at room temperature, in single path configuration referenced against a prerecorded baseline of water, all in the same 1-cm quartz cuvette. Between each pH measurement, stability of pH within the last digit of the pH meter for 2 min was required and, for every titration, the cuvette was cleaned with distilled water which was evaporated using nitrogen gas.

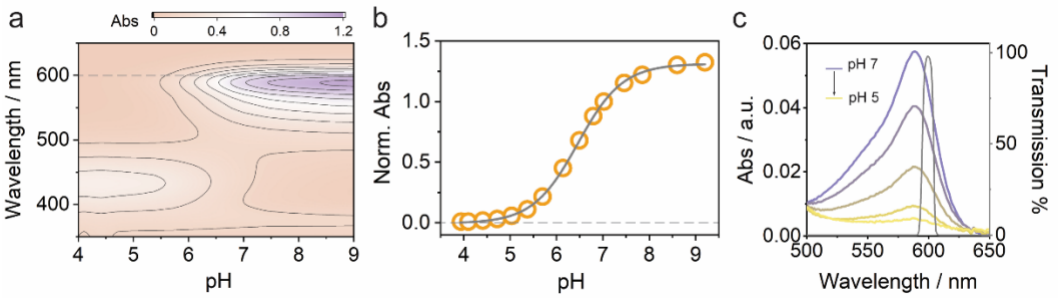

Figure S8. a) Absorption of BCP presented as a 2D color map as a function of probe wavelength along y and pH along x; **b)** pH dependence of the steady-state absorption of BCP at 600 nm, fitted using the function: pH = -0.48 * log(1.6e-6 * (-1 + 1.3 / (0.0055 + ratio))), ratio: A(pH)/A(pH=7); **c)** Absorbance decrease of BCP at 600 nm when varying pH from 7 to 5 (7.0, 6.5, 6.0, 5.5, 5.0). The gray line indicates the transmission regions of the 600-nm bandpass filter used in the measurement (nominal spectrum from THORLABS).

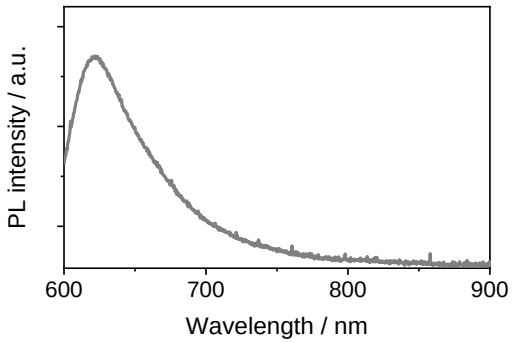

Figure S9. The emission spectra of BCP in H_2O acquired upon 580-nm excitation.